International Forum on Aeroelasticity and Structural Dynamics
IFASD 2017
25-28 June 2017 Como, Italy

QUANTITATIVE AEROELASTIC STABILITY EVALUATION OF CONTROL SURFACES WITH STRUCTURAL NONLINEARITIES

Aykut Tamer[*,1] **and Pierangelo Masarati**[**,1]

[1]Department of Aerospace Science and Technology
Politecnico Di Milano
via La Masa, 34 Milano 20156 Italy
[*]aykut.tamer@polimi.it, [**]pierangelo.masarati@polimi.it

Keywords: Stability, Lyapunov Exponents, Control System Nonlinearities

Abstract: This work discusses the quantitative stability evaluation of aeroelastic problems with nonlinearities in the control surfaces. Stability estimation of linear time invariant and linear time periodic systems rely on eigenanalysis of state transition matrices and implies simplifications on the problems governed by nonlinear non-autonomous equations. Lyapunov Characteristic Exponents directly provide quantitative information on the stability of nonlinear non-autonomous dynamical systems. Stability estimation using Lyapunov Characteristic Exponents does not require a special reference solution and is consistent with the eigensolution of linear time invariant and Floquet-Lyapunov analysis of linear time periodic systems. Thus, they represent a natural generalization of conventional stability analysis. The Discrete QR method is used to practically estimate the Lyapunov Characteristic Exponents. The method is applied to two- and three-dimensional aeroelastic problems with lumped nonlinearities in control surfaces.

1 INTRODUCTION

The aeroelasticity of linear systems is well addressed in literature (see Ref. [1] for the classical treatment of aeroelastic problems). On the other hand, nonlinearities in aeroelastic systems are often non-negligible and can be induced by structure, aerodynamics, and control systems. Nonlinearities introduce unique phenomena that cannot be predicted using linear system theory. Among them, limit cycle oscillations (LCO) occur as self sustained oscillations without the need of an external input [2] and there exist more complex behaviours such as bifurcations and chaos [3]. Many experiments on aeroelastic systems report phenomena of these kind; thus, it is crucial to understand and analyze nonlinear effects in aeroelastic systems for safe, efficient and improved designs of lifting and control surfaces [4].

Nonlinear aeroelasticity can be analyzed using theoretical and numerical methods, experimenting in wind tunnel and doing flight tests [5]. However, the practical, quantitative way of measuring stability depends on whether a system is autonomous (i.e. not explicitly dependent on time) and linear. Stability of linear, time invariant (LTI) problems can simply be inferred by evaluating the real part of the eigenvalues of its (constant) state space matrix, namely its spectrum. Stability evaluation is less straightforward when the problem is linear non-autonomous (i.e. explicitly dependent on time). According to Floquet-Lyapunov's theory, when the problem is time periodic (LTP), i.e. the state space matrix has periodic coefficients, the real part of the logarithm of the state transition matrix over one period. For nonlinear, autonomous problems, the eigenvalues and eigenvectors of the linearized system computed at the coordinates of the

phase plane corresponding to a steady solution provide local information about stability in the neighborhood of that solution. Once these points are evaluated and connected for the whole phase plane, a geometric and qualitative understanding of the system is possible. However, for non-autonomous problems and systems having higher dimensions, geometric understanding is not easy; thus, a quantitative measure is necessary.

In addition to difficulties in stability estimation of nonlinear systems, both LTI and LTP system analysis find several applications in mechanics and specifically in aerospace engineering. LTI and LTP problems typically result from linearization of nonlinear, non-autonomous problems about a steady (both LTI and LTP) or a periodic (LTP only) reference solution, which is called 'orbit'. Such linearization requires the existence of the reference solution, and the capability to define and compute it. Obtaining a steady or periodic solution by numerical integration in time requires that solution to be stable, so the study of the stability of the solution is actually the study of its stability margin.

A method that does not require a special reference solution (i.e. a stable point or a stable orbit) but, on the contrary, provides indications about the existence of an *attractor*, being it a point, a periodic orbit or a higher-order solution (e.g. a multidimensional torus), while computing the evolution of the system towards it, would give valuable insight into the system properties and, at the same time, provide a viable and practical means for its analysis. Lyapunov Characteristic Exponents (LCE) or in short Lyapunov Exponents are indicators of the nature and of the stability properties of solutions of differential equations (see for example Refs. [6, 7] and references therein). They define the spectrum of the related Cauchy (initial value) problem [8]. Lyapunov's theory can be applied to nonlinear, non-autonomous systems of differential equations. The stability of trajectories in state space can be estimated while computing their evolution.

In nonlinear aeroelasticity LCEs is used as a definitive method in estimating stability [5]. The LCEs estimation based on the time series chaos are studied in literature such as Ref. [9] studied the estimation LCEs from time series. Refs. [10, 11] investigated the aeroelastic response of an airfoil with structural nonlinearities; LCOs and chaotic motion is determined and compared with findings of Lyapunov Exponents obtained using time series analysis. In another work, aerodynamic and physical nonlinearities are studied for an airfoil in supersonic flow by Librescu et. al. [12], a criterion based on First Lyapunov Quantity is used to indicate bifurcations. The LCE indication of stability, which works directly on system differential equation rather than time series, has been recently applied to rotorcraft stability analysis in Ref. [13]; successful quantitative indications of the presence and stability of nonlinear phenomena could be obtained. Analytical sensitivity of LCEs is also considered in Ref. [14]. The possibility to extend the approach to systems of differential-algebraic equations, as outlined for example in Refs. [15–17], represents a promising development in view of their use in the formulation of modern multibody dynamics.

In this work we focus on quantitative stability estimation of aeroelastic problems involving nonlinearities that are often found in control surfaces. LCEs are implemented along with the governing differential equations and state transition matrix of the system rather than working on time series. Discrete QR method is used for LCE estimation. The next section introduces the stability problem of nonlinear systems and Lyapunov characteristic exponents (LCEs). Then, two nonlinear aeroelastic problems are presented and stability is estimated using LCEs and verified using time marching analysis.

2 STABILITY OF NONLINEAR PROBLEMS

This section recalls the definition of non-autonomous problems and of Lyapunov Characteristic Exponents as measures of their spectrum, along with numerical procedures for their estimation.

2.1 Nonlinear, Non-Autonomous Problems

In engineering practice, differential problems of the form

$$\dot{\mathbf{x}} = \mathbf{f}\left(\mathbf{x}, t\right), \qquad \mathbf{x}(t_0) = \mathbf{x}_0 \tag{1}$$

often arise. Special cases occur when the problem is linear, i.e. $\mathbf{f}(\mathbf{x}, t) = \mathbf{A}(t)\mathbf{x}(t)$, and particularly time-periodic (LTP), i.e. linear with $\mathbf{A}(t+T) = \mathbf{A}(t)$ for a given constant T, $\forall t$, or time-invariant (LTI), i.e. linear, with $\mathbf{A}$ independent of time. Autonomous problems arise when $\mathbf{f}(\mathbf{x})$ does not explicitly depend on time t; when the problem is linear, i.e. $\mathbf{f}(\mathbf{x}) = \mathbf{A}\mathbf{x}$, with $\mathbf{A}$ constant, they yield the LTI case again. Stability of linear, time invariant (LTI) problems

$$\dot{\mathbf{x}} = \mathbf{A}\mathbf{x} \tag{2}$$

can simply be inferred by evaluating the real part of the eigenvalues of its (constant) state space matrix $\mathbf{A}$, namely its spectrum. Stability evaluation is less straightforward when the problem is linear non-autonomous. According to Floquet-Lyapunov's theory, when the problem is time periodic (LTP), i.e. the state space matrix has periodic coefficients,

$$\dot{\mathbf{x}} = \mathbf{A}(t)\mathbf{x}, \qquad \mathbf{A}(t+T) = \mathbf{A}(t)\,\forall t, \tag{3}$$

the stability of LTP systems is evaluated using the real part of the logarithm of the eigenvalues of the monodromy matrix $\mathbf{H}$, namely the state transition matrix $\mathbf{Y}$ over one period (T):

$$\mathbf{H} = \mathbf{Y}(T, 0), \tag{4}$$

which is the solution of the problem

$$\dot{\mathbf{Y}} = \mathbf{A}(t)\mathbf{Y}, \qquad \mathbf{Y}(0) = \mathbf{I}. \tag{5}$$

Although the definition of stability may be less intuitive for time dependent and nonlinear problems, the rate of decay of the amplitude of the trajectory with respect to initial perturbations, i.e. its *stability*, has the same interpretation, and all cases are quantitatively comparable. Stability indicators are the real part of the eigenvalues of matrix $\mathbf{A}$ for LTI systems, the logarithm of the real part of the eigenvalues of the monodromy matrix for LTP problems. As discussed in the next chapter, the Lyapunov Characteristic Exponents is the generalization of linear eigenanalysis for nonlinear and non-autonomous systems.

2.2 Lyapunov Characteristic Exponents

Given the problem $\dot{\mathbf{x}} = \mathbf{f}(\mathbf{x}, t)$, with the state $\mathbf{x} \in \mathbb{R}^n$, the time $t \in \mathbb{R}$, and the nonlinear function $\mathbf{f} \in \mathbb{R}^{n+1} \to \mathbb{R}^n$, and a solution $\mathbf{x}(t)$ for given initial conditions $\mathbf{x}(t_0) = \mathbf{x}_0$, the Lyapunov Characteristic Exponents λ_i are defined as:

$$\lambda_i = \lim_{t\to\infty} \frac{1}{t} \log \left\| {}_i\mathbf{x}(t) \right\|, \tag{6}$$

where, as presented in Fig. 1, ${}_i\mathbf{x}(t)$ is the solution that describes the exponential evolution of the i-th axis of the ellipsoid that grows from an initially infinitesimal n-sphere according to the map $\mathbf{f}_{/\mathbf{x}}$ tangent to $\mathbf{f}$ along the fiducial trajectory $\mathbf{x}(t)$. In other words, ${}_i\mathbf{x}(t)$ is the solution of the linear, non-autonomous problem ${}_i\dot{\mathbf{x}}(t) = \mathbf{f}_{/\mathbf{x}}(\mathbf{x}(t), t)\,{}_i\mathbf{x}(t)$, with ${}_i\mathbf{x}(t_0) = {}_i\mathbf{x}_0$. The definition involves the limit for $t \to \infty$; hence, in practice LCEs can only be numerically estimated for a sufficiently large value of t. In this study, the term "LCEs" indicate their (numerical) estimation using a large enough value of t, such that the convergence is satisfied.

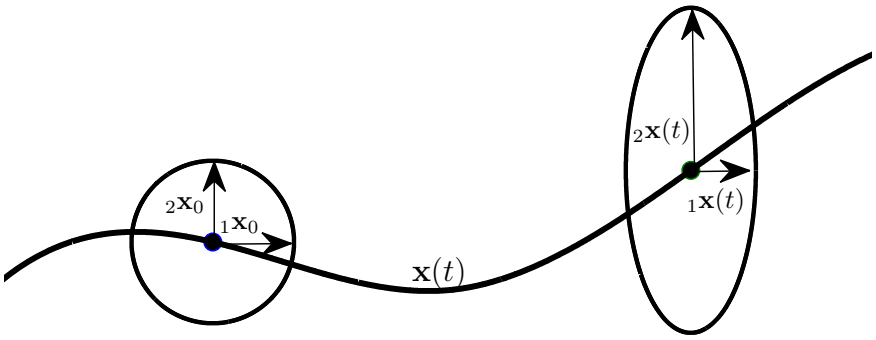

Figure 1: Evolution of the solution of a differential equation

LCEs represent a measure of the rate of growth of perturbed solutions. Consider infinitesimal, independent perturbations of the states with respect to a solution $\mathbf{x}(t)$ of Eq. (6) (the fiducial trajectory). The perturbed solution can be computed in terms of the state transition matrix $\mathbf{Y}(t, t_0)$, considering $\mathbf{A}(\mathbf{x}, t) = \mathbf{f}_{/\mathbf{x}}$, as the solution of the problem

$$\dot{\mathbf{Y}}(t, t_0) = \mathbf{A}(\mathbf{x}, t)\mathbf{Y}(t, t_0), \qquad \mathbf{Y}(t_0, t_0) = \mathbf{I}. \tag{7}$$

According to the Ostrogradskiĭ-Jacobi-Liouville formula [6], the determinant of $\mathbf{Y}(t, t_0)$ (the *Wronskian determinant* of the independent solutions that constitute $\mathbf{Y}(t, t_0)$) is

$$\det\left(\mathbf{Y}(t, t_0)\right) = \det\left(\mathbf{Y}(t_0, t_0)\right) \mathrm{e}^{\int_{t_0}^{t} \mathrm{tr}(\mathbf{A}(\tau))\ \mathrm{d}\tau}, \tag{8}$$

where $\mathrm{tr}(\cdot)$ is the trace operator. Thus, the Wronskian never vanishes when $\mathbf{A}(t)$ is regular in $[t_0, t]$, since $\mathbf{Y}(t_0, t_0) \equiv \mathbf{I}$. The Wronskian geometrically represents the evolution in time of the volume of an infinitesimal portion of the state space.

LCEs estimation suffer from the numerical difficulty of dealing with matrices whose coefficients either rapidly converge to zero (exponential stability) or diverge (instability). For this reason, different approaches have been formulated. Continuous formulations for the estimation of the LCEs can be derived from the definition based on the singular value decomposition (SVD), or on the QR decomposition (see for example Ref. [18]). A recent and ongoing investigation also considered Schur decomposition in case of multiple LCEs [19]. The discrete QR method, based on the incremental use of the QR decomposition of the state transition matrix for each time step, is used in this study and discussed in the next section.

2.3 The Discrete QR Method

One of the most popular methods of LCE estimation is the Discrete QR Method, which is based on incrementally updating the LCEs estimates with the diagonal elements of the upper-triangular matrix $\mathbf{R}$ obtained from the QR decomposition of the state transition matrix between two consecutive time steps.

Given the previously defined state transition matrix $\mathbf{Y}(t, t_{j-1})$ from time t_{j-1} to an arbitrary time t, set $\mathbf{Y}_j = \mathbf{Y}(t_j, t_{j-1})$. Consider then the QR decomposition of $\mathbf{Y}_j\mathbf{Q}_{j-1}$, starting from $\mathbf{Q}_0 = \mathbf{I}$, which implies $\mathbf{Q}_j\mathbf{R}_j = \mathbf{Y}_j\mathbf{Q}_{j-1}$. After defining $\mathbf{R}_{\Pi_j} = \Pi_{k=0}^{j}\mathbf{R}_{j-k}$, one can show that

$$\mathbf{Y}_j\mathbf{Q}_{j-1}\mathbf{R}_{\Pi_{j-1}} = \mathbf{Q}_j\mathbf{R}_j\mathbf{R}_{\Pi_{j-1}} = \mathbf{Q}_j\mathbf{R}_{\Pi_j} \tag{9}$$

This way, $\mathbf{Y}_j\mathbf{Q}_{j-1}\mathbf{R}_{\Pi_{j-1}}$ can be used to construct $\mathbf{R}_{\Pi_j}$ by considering incremental QR decompositions over $\mathbf{Y}_j\mathbf{Q}_{j-1}$, i.e. with limited contraction/expansion. The LCEs are then estimated from $\mathbf{R}_{\Pi_j}$ as

$$\lambda_i = \lim_{j\to\infty} \frac{1}{t_j} \log r_{ii}(t_j), \tag{10}$$

where $r_{ii}(t_j)$ are the diagonal elements of matrix $\mathbf{R}(t_j) = \mathbf{R}_{\Pi_j}$. It is worth noticing that the product of two upper triangular matrices $\mathbf{C} = \mathbf{AB}$ is also an upper triangular matrix, whose diagonal elements are $c_{ii} = a_{ii}b_{ii}$. Thus the logarithm of c_{ii} can be incrementally computed as $\log(a_{ii}b_{ii}) = \log(a_{ii}) + \log(b_{ii})$, which helps preventing overflow/underflow in numerical computations. Furthermore,

$$r_{ii}(t_j) = \Pi_{k=0}^{j} r_{(j-k)_{ii}}, \text{ thus } \log\left(r_{ii}(t_j)\right) = \sum_{k=0}^{j} \log(r_{k_{ii}}), \tag{11}$$

which leads to

$$\lambda_i = \lim_{j\to\infty} \frac{1}{t_j} \sum_{k=0}^{j} \log(r_{k_{ii}}). \tag{12}$$

3 APPLICATIONS

This section presents the quantitative stability evaluation of two aeroelastic problems, which are numerically and experimentally analyzed in the literature as examples of aeroelastic systems with lumped structural nonlinearities. To compare the findings of the original studies with the indications coming from LCEs, system parameters and unsteady aerodynamic models are kept the same. The first example is related to a cubic representation of the restoring pitch moment of an airfoil, which can be seen as a simplification of an aileron or elevator. The second application considers a two dimensional representation of a wing-aileron system, with the joint between two possesses freeplay. For both examples, Fig. 2 presents a generic layout of the cross section of a wing with span s and chord length $2b$, with the degrees of freedom of pitch, α, plunge, h, and flap, β. The degrees of freedom are constrained with spring k and dampers c.The dimensions are normalized by semi-chord length b and include: position of elastic axis a, center of gravity x_α, position of the flap hinge c. The mass of the wing is represented by m_W, total mass including wing and support is denoted by m_T. S and I refer to the first and second moment of mass with respect to the hinges. In the equations subscripts α and β indicate the parameters corresponding to that motion.

3.1 Mathematical Model

The mathematical representation of an aeroelastic airfoil motion is given in Ref. [20]. For the linear model, the mass, stiffness and damping matrices of the model in-vacuo are given in non-dimensional form as:

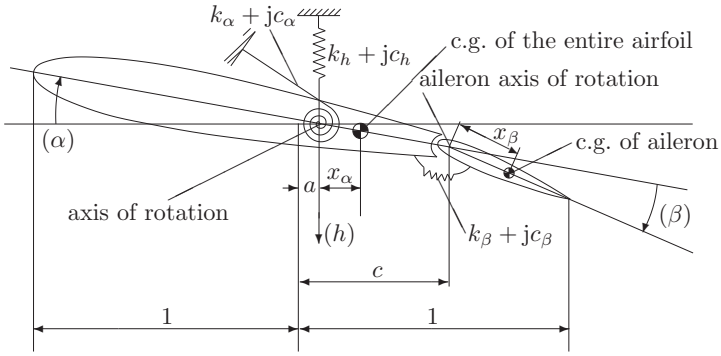

Figure 2: Airfoil with aileron: Aeroelastic Model of the pitch-plunge-flap systems, non-dimensionalized with semi-chord length b

$$\mathbf{M_s} = \begin{bmatrix} r_\alpha^2 & r_\beta^2 + (c-a)x_\beta & x_\alpha \\ r_\beta^2 + (c-a)x_\beta & r_\beta^2 & x_\beta \\ x_\alpha & x_\beta & M_T/m_W \end{bmatrix} \tag{13a}$$

$$\mathbf{K_s} = \begin{bmatrix} r_\alpha^2\omega_\alpha^2 & 0 & 0 \\ 0 & r_\beta^2\omega^2\beta & 0 \\ 0 & 0 & \omega_h^2 \end{bmatrix} \tag{13b}$$

$$\mathbf{D_s} = \begin{bmatrix} 2\omega_\alpha\xi_\alpha & 0 & 0 \\ 0 & 2\omega_\beta\xi_\beta & 0 \\ 0 & 0 & 2\omega_h\xi_h \end{bmatrix} \tag{13c}$$

where the non-dimensional parameters are defined as:

$$x_\alpha = \frac{S_\alpha}{m_W b},\ \ x_\beta = \frac{S_\beta}{m_W b},\ \ r_\alpha^2 = \frac{I_\alpha}{m_W b^2},\ \ r_\beta^2 = \frac{I_\beta}{m_W b^2} \tag{14a}$$

$$\omega_\alpha = \sqrt{\frac{k_\alpha}{I_\alpha}},\ \ \omega_\beta\sqrt{\frac{k_\alpha}{I_\alpha}},\ \ \omega_h = \sqrt{\frac{k_h}{m_T}},\ \ \xi_\alpha = \frac{c_\alpha}{2m_W\omega_\alpha},\ \ \xi_\beta = \frac{c_\beta}{2I_\beta\omega_\beta},\ \ \xi_h = \frac{c_h}{2m_W\omega_h} \tag{14b}$$

The unsteady aerodynamic formulation follows a set of functions T_j, introduced by Theodorsen and Garrick [21]. For the pitch-plunge-flap system of Fig. 2, the vertical force P, and hinge moments M_α and M_β can be obtained from Ref. [21] as:

$$P = -\rho b^2\left(\pi\ddot{h} + U\pi\dot{\alpha} - \pi ba - \ddot{\alpha} - UT_4\dot{\beta} - T_1 b\ddot{\beta}\right) - 2\pi\rho UbC(k)Q \tag{15a}$$

$$\begin{aligned} M_\alpha = &-\pi b^2\Bigg[-a\pi b\ddot{h} + \pi\left(\frac{1}{2}-a\right)Ub\dot{\alpha} - \left(\frac{1}{8}+a^2\right)\ddot{\alpha} \\ &+ T_{15}U^2\beta + T_{16}Ub\dot{\beta} + 2T_{12}b^2\ddot{\beta}\Bigg] + 2\pi\rho Ub^2\left(a+\frac{1}{2}\right)C(k)Q \end{aligned} \tag{15b}$$

$$\begin{aligned} M_\beta = &-\rho b^2\left(-T_1 b\ddot{h} + T_{17}Ub\dot{\alpha} + 2T_{12}b^2\ddot{\alpha} + \frac{T_{13}}{\pi}U^2\beta + \frac{T_{19}}{\pi}Ub\dot{\beta} - \frac{T_3}{\pi}b^2\ddot{\beta}\right) \\ &- \rho Ub^2T_{12}C(k)Q \end{aligned} \tag{15c}$$

$$Q = U\alpha + \dot{h} + b\left(\frac{1}{2}-a\right)\dot{\alpha} + \frac{U}{\pi}T_{10}\beta + \frac{b}{2\pi}T_{11}\dot{\beta} \tag{15d}$$

where ρ is the air density, $C(k)$ is lift deficiency function as a function of reduced frequency k and T functions are derived in Ref. [21]. As explained in Ref. [1], for arbitrary airfoil motions starting from rest, the term $C(k)Q$ multiplication can be written using superposition integral as:

$$c(k)Q = Q(0)\phi(\tau) + \int_0^\tau \frac{dQ(\sigma)}{d\sigma}\phi(\tau-\sigma)d\sigma \tag{16}$$

where $\phi(\tau)$ is the Wagner function. An approximation is given as [1]:

$$\phi(\tau) \approx c_0 - c_1 e^{-c_2\tau} - c_3 e^{-c_4\tau} \tag{17}$$

with $c_0 = 1$ $c_1 = 0.165$ $c_2 = 0.0455$ $c_2 = 0.335$ and $c_4 = 0.3$.

Ref. [20] used the approximated Wagner's function and two augmented states to obtain the unsteady aerodynamics in matrix form. First, the non-circulatory terms aerodynamic mass, damping and stiffness matrices are given as:

$$\frac{\mathbf{M_{NC}}}{-\frac{\rho b^2}{m_W}} = \begin{bmatrix} \pi\left(\frac{1}{8}+a^2\right) & -(T_7+(c-a)T1) & -\pi a \\ 2T_{13} & -T_3/\pi & -T_1 \\ -\pi a & -T_1 & \pi \end{bmatrix} \tag{18a}$$

$$\frac{\mathbf{D_{NC}}}{-\frac{\rho U b}{m_W}} = \begin{bmatrix} \pi\left(\frac{1}{2}-a\right) & T_{1s}-(c-a)T_4 & 0 \\ T_{2s}+T_4\left(a-\frac{1}{2}\right) & -T_4T_{11}/(2\pi) & 0 \\ \pi & -T_4 & 0 \end{bmatrix} \tag{18b}$$

$$\frac{\mathbf{K_{NC}}}{-\frac{\rho U^2}{m_W}} = \begin{bmatrix} 0 & T_4+T_{10} & 0 \\ 0 & (T_5-T_4T_10)/\pi & 0 \\ 0 & 0 & 0 \end{bmatrix} \tag{18c}$$

Then these non-circulatory aerodynamic matrices are summed with structural and circulatory aerodynamics matrices and and overall mass damping and stiffness matrices are obtained as:

$$\mathbf{M_t} = \mathbf{M_s} - \mathbf{M_{NC}} \tag{19a}$$

$$\mathbf{D_t} = \mathbf{D_s} - \mathbf{D_{NC}} - \frac{1}{2}\mathbf{RS_1} \tag{19b}$$

$$\mathbf{K_t} = \mathbf{K_s} - \mathbf{K_{NC}} - \frac{1}{2}\mathbf{RS_2} \tag{19c}$$

$$\mathbf{D} = \mathbf{RS_3} \tag{19d}$$

where:

$$\mathbf{R} = -\frac{\rho U}{m_W}\begin{bmatrix} \left(a+\frac{1}{2}\right) & -T_{12} & -2\pi \end{bmatrix}^T \tag{20a}$$

$$\mathbf{S_1} = \begin{bmatrix} U & T_{10}U/\pi & 0 \end{bmatrix} \tag{20b}$$

$$\mathbf{S_2} = \begin{bmatrix} b\left(\frac{1}{2}-a\right) & bT_{11}U/2\pi & b \end{bmatrix} \tag{20c}$$

$$\mathbf{S_3} = \begin{bmatrix} c_2c_4(c_1+c_3)U^2/b & (c_1c_2+c_3C_4)U \end{bmatrix} \tag{20d}$$

$$T_{1s} = T_1 - T_8 + T_{11}, \;\; T_{2s} = -2T_9 - T_1 \tag{20e}$$

Now the state variables vector $\mathbf{x}$ includes both physical variables of pitch, flap and plunge and two augmented aerodynamic states:

$$\mathbf{x} = \left[\begin{array}{cccccccc} \alpha & \beta & h/b & \dot{\alpha} & \dot{\beta} & \dot{h}/b & \bar{x} & \dot{\bar{x}} \end{array} \right]^T. \tag{21}$$

where the augmented states are related to the physical system variables according to:

$$\ddot{\bar{x}} = -c_2 c_4 \frac{U^2}{b^2}\bar{x} - (c_2 + c_4)\frac{U}{b}\dot{\bar{x}} + \frac{U}{b}\alpha + \left(\frac{1}{2} - a\right)\dot{\alpha} + \frac{\dot{h}}{b} \tag{22}$$

The nonlinear problem can then be defined as a multiplication of a linear problem and a nonlinear forcing function:

$$\dot{\mathbf{x}} = \mathbf{A}\mathbf{x} + \mathbf{g} \tag{23}$$

where state space matrix $\mathbf{A}$ and nonlinear forcing function $\mathbf{g}$ are given as:

$$\mathbf{A} = \left[\begin{array}{ccc} \mathbf{0} & \mathbf{I} & \mathbf{0} \\ -\mathbf{M_t}^{-1}\mathbf{K_t} & -\mathbf{M_t}^{-1}\mathbf{D_t} & \mathbf{M_t}^{-1}\mathbf{D} \\ \mathbf{E_1} & \mathbf{E_2} & \mathbf{F} \end{array} \right], \quad \mathbf{g} = \left[\begin{array}{c} \mathbf{0} \\ -\mathbf{M_t}^{-1}\mathbf{f}_{nl}(\mathbf{x}, t) \\ \mathbf{0} \end{array} \right] \tag{24}$$

for the following set of sub-matrices corresponding to the augmented states:

$$\mathbf{E_1} = \left[\begin{array}{ccc} 0 & 0 & 0 \\ \frac{U}{b} & \frac{UT_{10}}{\pi b} & 0 \end{array} \right], \quad \mathbf{E_2} = \left[\begin{array}{ccc} 0 & 0 & 0 \\ \frac{1}{2} - a & \frac{T_{11}}{2\pi} & 0 \end{array} \right], \quad \mathbf{F} = \left[\begin{array}{cc} 0 & 1 \\ -\frac{c_2 c_4 U^2}{b^2} & -\frac{(c_2 + c_4)U}{b} \end{array} \right] \tag{25}$$

The nonlinear function $\mathbf{f}_{nl}$ depends on the type of the nonlinearity and separately described within the examples.

3.2 Spring with Cubic Stiffness

The cubic spring is characterized by the presence of a quadratic term in the stiffness coefficient [4]. In the literature, this problem has been investigated numerically and experimentally to determine the effects of the cubic spring on the aeroelastic stability of airfoils. Depending on the characteristics of the cubic spring, namely a soft or a hard one, the flutter characteristics of the system can change significantly and depend on the initial conditions [22]. It is also observed that limit cycle oscillations (LCOs) is a common consequence of a cubic restoring moment (See for example Refs. [10, 23–25]).

In order to compare the agreement between LCEs estimation and the response of a system with a cubic stiffness nonlinearity, the 2D aeroelastic model of Ref. [24] is used. The numerical values reported therein are given in Table 1. The model includes plunge and pitch degrees of freedom, with center of mass and elastic axis offset from the rotation axis; this corresponds to the model of Fig. 2 without the aileron ($c = 1$).

The torsional spring coefficient $k_\alpha(\alpha)$ that resists the pitch motion is mathematically represented by a quadratic function:

$$k(\alpha) = k_{\alpha 1}\alpha + k_{\alpha 2}\alpha^2 \tag{26}$$

Variable Description	Value
Span, s	0.6 m
Semi-chord, b	0.0325 m
Position of elastic axis normalized by semi-chord, a	-0.5
Center of gravity normalized by semi-chord, x_α	0.5
Air density, ρ	1.225 kg/m^3
Mass of the wing, m_W	1.0662 kg
Mass of wing and supports, m_T	3.836 kg
Moment of inertia about the elastic axis, I_α	4067.5 N m s rad^{-1}
Pitch and plunge damping coefficients, c_α, c_h	0.0115, 0.011 kgm^2/s
Stiffness in pitch and plunge, $k_{\alpha 0}$, k_h	0.942, 895.10 N m^{-1}
Stiffness constants of nonlinear damper, $k_{\alpha 1}$, $k_{\alpha 2}$	3.95, 107 N m

Table 1: Cubic stiffness: Section parameters

where the nonlinear terms $k_{\alpha 1} = 3.95$ N m and $k_{\alpha 2} = 107$ N m are estimated in Ref. [24] based on the comparison of the analytical and experimental results of the airfoil motion. The nonlinear forcing function corresponding to Eq. 24 is then:

$$\mathbf{f}_{nl} = \begin{bmatrix} (k_{\alpha 1}\alpha + k_{\alpha 0}\alpha^2)\alpha & 0 & 0 \end{bmatrix}^T \tag{27}$$

A reduced model can then be obtained by removing flap degree of freedom from the matrices of governing equations of motion mentioned from Eq. 13 to 25. Tracking the real part of the eigenvalues of state space matrix $\mathbf{A}$ of Eq. 23 with flight speed gives the flutter speed of the linear model and is numerically found to be $U_f = 10.90$ m s^{-1}, which is in agreement with the results of Ref. [24], details are skipped here. For the two air-stream values above flutter speed at $U = 1.25U_f$ and $U = 1.40U_f$, pitch response of the nonlinear system is presented in Figs. 3 and 4 respectively, along with the corresponding non-dimensional phase plane plots, which indicate the topological properties of the state space. The initial configuration in the phase plane plots are marked with a solid dot. It should be noted here that only pitching motion is shown here; the intersections observed in the plots are due to projection of the variable and its time derivative on a 2D plane.

When the airstream speed exceeds the flutter speed for a linear system, any perturbation from its equilibrium condition would lead to a divergent response. As a consequence of nonlinearity in stiffness however, the system experiences oscillatory motion; the phase portrait converges to an orbit regardless of the initial condition, thus an LCO occurs. This is illustrated in Figs. 3 and 4 for flight speeds of $U = 1.25U_f$ and $U = 1.40U_f$. The amplitude and phase portraits of the responses are in agreement with those of Ref. [24]. The periodic orbits of Figs. 3 and 4 are of particular interest. When a nonlinear system has a periodic attractor (for example a LCO), zero-valued largest LCE estimates (or very close to zero from a numerical analysis point of view) are expected [26]. This can be observed in Fig. 5(a) and Fig. 5(b), which present the time evolution of LCEs for the corresponding flight speed values of $U = 1.25U_f$ and $U = 1.40U_f$. The largest LCE branch converges to zero, while the other tends to be a negative value. Thus, the LCE estimates are compatible with the periodic motion of the system shown in Figs. 3 and 4. Note that for $U = 1.40U_f$, the LCE estimation converges slower and the separation $(\lambda_1 - \lambda_1)$ between the two LCEs increases approximately from 0.20 to 0.30.

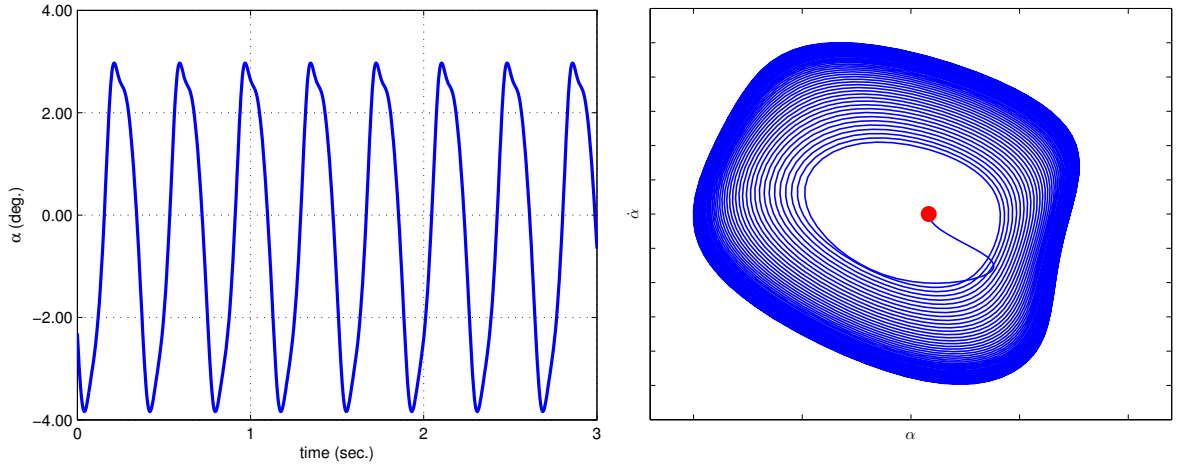

(a) time history (b) non-dimensional phase plot

Figure 3: Cubic stiffness: Time history and normalized phase plot of pitch motion after a perturbation, $U = 1.25U_f$

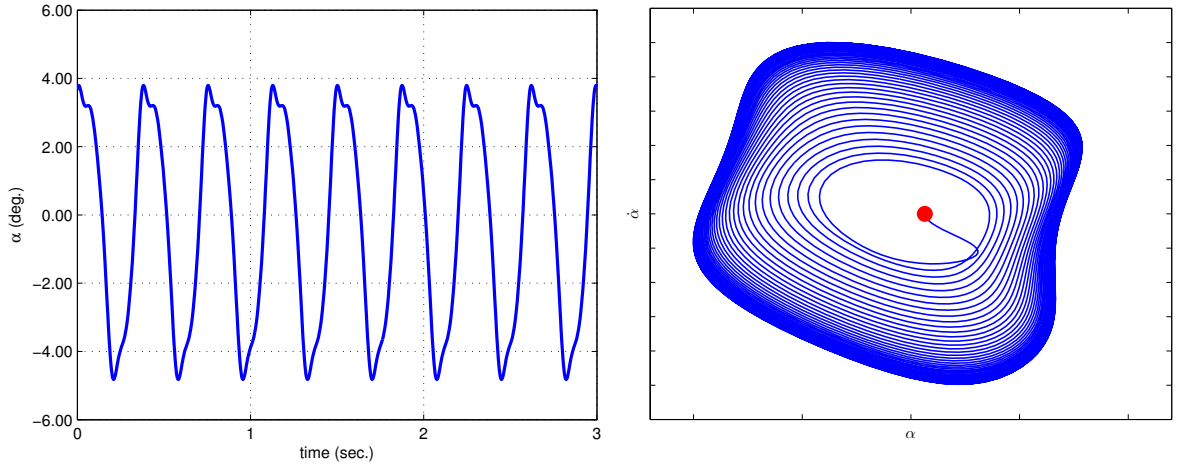

(a) time history (b) non-dimensional phase plot

Figure 4: Cubic stiffness: Time history and normalized phase plot of pitch motion after a perturbation, $U = 1.40U_f$

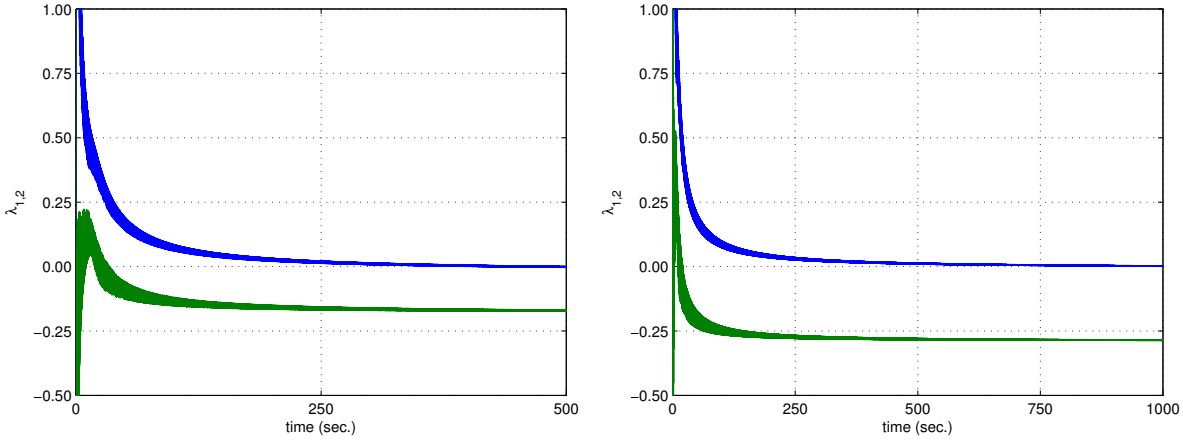

(a) $U = 1.25U_f$ (b) $U = 1.40U_f$

Figure 5: Cubic stiffness: Time evolution of LCEs, $U = 1.25U_f$ (a) and $U = 1.40U_f$ (b)

3.3 Airfoil Dynamics with Freeplay in Aileron

Control surface hinges often exhibit freeplay [4], which may possibly result in instability or self-excited LCO, and chaotic or quasi-periodic motion. When the position of a control system falls in the freeplay region, the control is disconnected from its actuation; it re-connects once the deflection of the control surface exceeds the freeplay limit [27]. While there exist numerical methods such as harmonic balance [28], a possible continuous and differentiable representation is possible using hyperbolic functions, as given in Ref. [29]:

$$f_h(\beta) = \frac{1}{2}k[1 - \tanh(\varepsilon(\beta - \beta_l))](\beta - \beta_l) + \frac{1}{2}k[1 - \tanh(\varepsilon(\beta - \beta_u))](\beta - \beta_u), \tag{28}$$

where β is the rotation of a generic control system degree of freedom corresponding to the flapping motion of Fig. 2, β_l and β_u are the lower and upper boundaries of the freeplay region, $\delta_{FP} = \beta_u - \beta_l$. The constant k is the stiffness of the control surface which is equal to $r_\beta^2\omega_\beta^2$ for the linear case. The parameter ε is tuned to better catch the real freeplay behavior. Then for this nonlinear case, hinge moment $f_h(\beta)$ is replaced with the corresponding nonlinear force of Eq. 24 and added to the right hand side as a forcing contribution:

$$\mathbf{f}_{nl} = \begin{bmatrix} 0 & f_h(\beta) & 0 \end{bmatrix}^T \tag{29}$$

This hyperbolic representation is implemented in Refs. [29] and [30] to introduce the freeplay discontinuity in an aeroelastic airfoil model; chaotic motion and LCOs are reported as a consequence. The mathematical representation of an aeroelastic airfoil dynamics given in Ref. [29] is used in this study; physically corresponding to the model presented in Fig. 2 with freeplay in the aileron hinge spring. System parameters of the 3D airfoil given in Ref. [31] are used and reported in Table 2.

Variable Description	Value
Span, s	0.52 m
Semi-chord, b	0.127 m
Position of elastic axis normalized by semi-chord, a	-0.5
Position of hinge line normalized by semi-chord, c	0.5
Center of gravity normalized by semi-chord, x_α	0.434
Center of gravity normalized by semi-chord, x_β	0.01996
Radius of gyration about the elastic axis per span, r_α	0.7321
Radius of gyration about the aileron hinge per span, r_β	0.11397
Pitching motion stiffness coefficient, k_α,	1486 1/s^2
Flapping motion stiffness coefficient, k_β,	155 1/s^2
Plunging motion stiffness coefficient, k_h,	1809 1/s^2
Air density, ρ	1.225 kg/m^3
Mass of the wing, m_W	0.62868 kg
Mass of the aileron, m_a	0.1859 kg
Mass of each of two supports, m_s	0.47485 kg
Pitching motion structural damping coefficient, $c_\alpha/2m_W\omega_\alpha$,	0.01626
Flapping motion structural damping coefficient, $c_\beta/2I_\beta\omega_\beta$,	0.0115
Plunging motion structural damping coefficient, $c_h/2m_W\omega_h$,	0.0113
Freeplay region, δ_{FP},	2.12 deg

Table 2: Freeplay in aileron: Section parameters

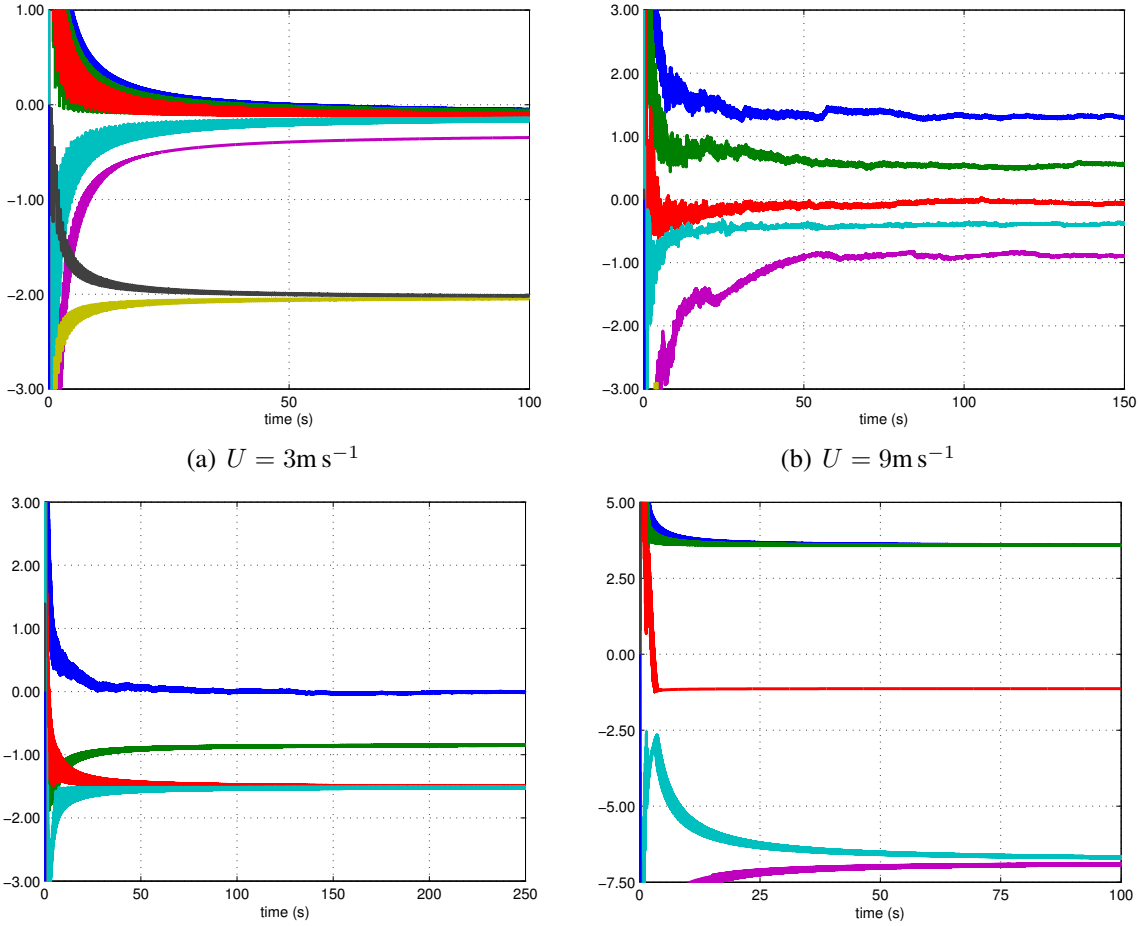

(a) $U = 3\text{m}\,\text{s}^{-1}$ (b) $U = 9\text{m}\,\text{s}^{-1}$

(c) $U = 18\text{m}\,\text{s}^{-1}$ (d) $U = 27\text{m}\,\text{s}^{-1}$

Figure 6: Freeplay in aileron: Time evolution of LCEs for: convergent response (a: $U = 3\text{m}\,\text{s}^{-1}$), chaotic response (b: $U = 9\text{m}\,\text{s}^{-1}$), periodic attractor (c: $U = 18\text{m}\,\text{s}^{-1}$) and divergent response (d: $U = 27\text{m}\,\text{s}^{-1}$)

By tracking the real part of the eigenvalues of state space matrix $\mathbf{A}$ of Eq. 23 with flight speed gives the flutter speed of the linear model, which is found to be approximately $23.9\ \text{m}\,\text{s}^{-1}$ and is in close agreement with the results of Refs. [29]. In Ref. [29], it is reported that the nonlinear system with freeplay in the aileron motion presents transitions in response characteristics, bifurcating from stable response at low flight speeds to chaos at mid to high speed. Close to the flutter speed, LCOs occur and, for velocities slightly higher than the linear flutter speed, divergent oscillations are observed. The quantitative stability analysis of these observed phenomena can be obtained using Lyapunov's theory. For illustrative purposes, each of these characteristic motions has been identified at some particular flight speeds for the aileron motion. The spectra of the nonlinear problems are obtained using LCEs. For each of these characteristic motions, the steady flapping motion and the time evolution of the LCE estimates are presented in Fig. 6. The relations between the qualitative behavior of the flapping motion and the corresponding quantitative LCE estimates are discussed.

At low speed, the nonlinear system is stable, with quickly vanishing oscillations. Fig. 7 shows the aileron motion and the non-dimensional phase plot after a perturbation at a flight speed of $3\ \text{m}\,\text{s}^{-1}$. For this case, the expected LCE spectrum is made of all negative values; this is confirmed by the time evolution of LCE estimates presented in Fig. 6(a): the largest LCE with its conjugate converges to a value slightly less than zero.

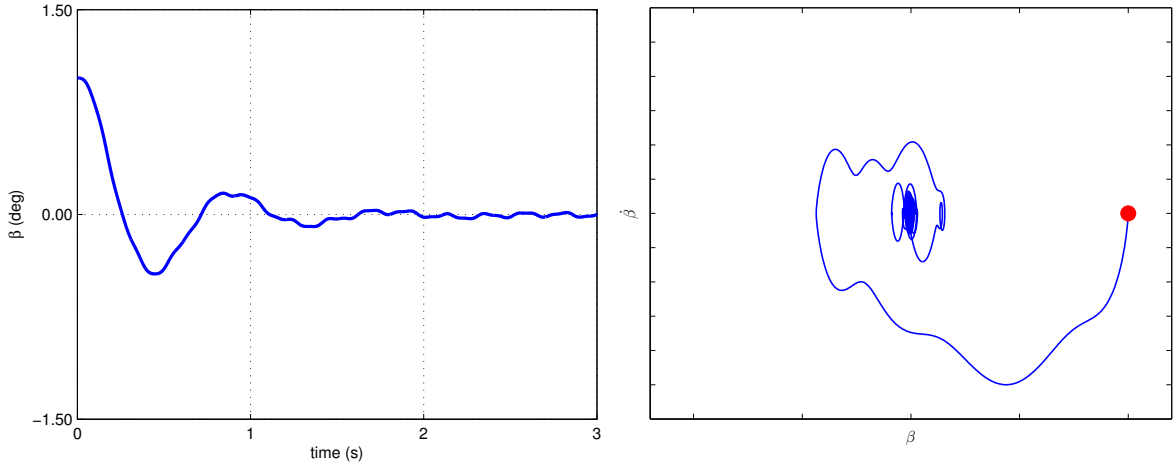

(a) time history (b) non-dimensional phase plot

Figure 7: Freeplay: aileron response at $U = 3\text{m}\,\text{s}^{-1}$; time history (a) and non-dimensional phase-plot (b)

At a larger airstream speed, the nonlinear system shows a transition from stable to random non-periodic motion, as illustrated in the time history of Fig. 8(a) at an airstream speed of 9 $\text{m}\,\text{s}^{-1}$, resulting in self-sustained arbitrary but bounded oscillations. The phase plot of Fig. 8(b) shows that the solution tends to visit all points in a bounded region of the phase plane. For a nonlinear system, a positive LCE indicates non-convergent trajectory, such as chaos [26]. Fig. 6(b) confirms this behaviour, showing two positive and separate LCEs.

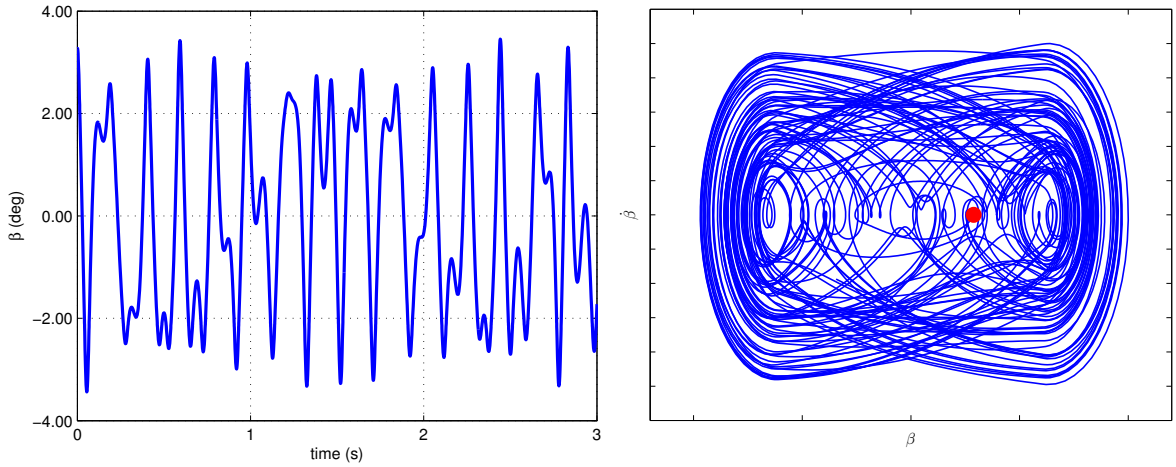

(a) time history (b) non-dimensional phase plot

Figure 8: Freeplay: aileron response at $U = 9\text{m}\,\text{s}^{-1}$; time history (a) and non-dimensional phase-plot (b)

In proximity of the flutter speed of the linear model, the amplitude of the oscillations increases; thus, the freeplay region is significantly exceeded. Two regions exist: one in the the freeplay region without restoring moment, where oscillations cannot be slowed down, and another in which a flexible restraint on the airfoil motion provides a sufficient level of moment to prevent divergence and arbitrarily large oscillations. This leads to a periodic orbit of the flapping motion in a self-sustained manner without the need of an external input, i.e. a LCO, as shown by the oscillatory motion of Fig. 9(a) and orbital phase plot of Fig. 9(b) at a flight speed of 18 $\text{m}\,\text{s}^{-1}$. When the solution has a periodic attractor, zero-valued LCE estimates (or very close to zero

from a numerical analysis point of view) are expected [26]. The quantitative indication of LCOs can be observed in Fig. 6(c), with the largest LCE converging to zero.

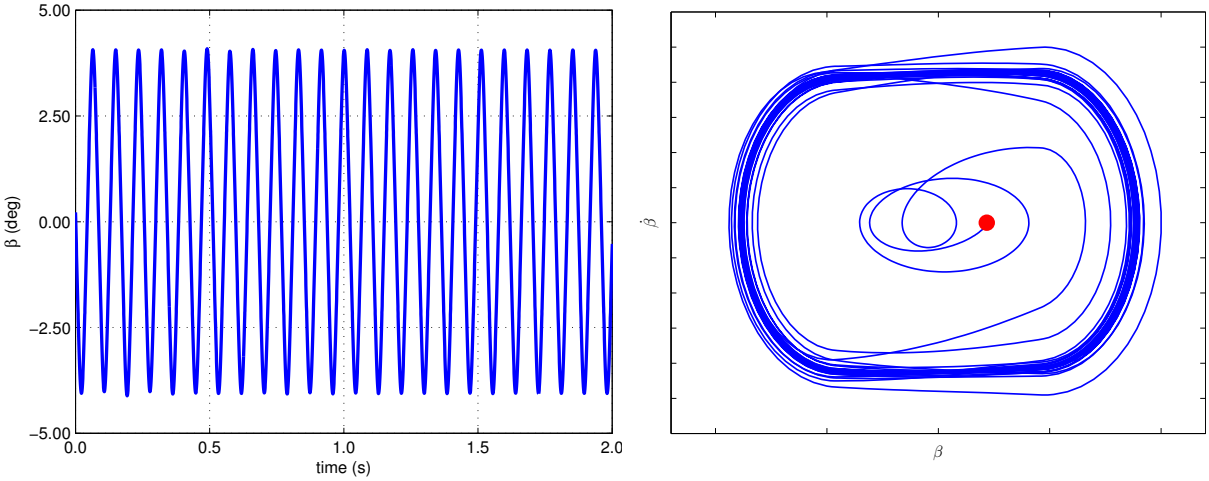

(a) time history (b) non-dimensional phase plot

Figure 9: Freeplay: aileron response at $U = 18\text{m}\,\text{s}^{-1}$; time history (a) and non-dimensional phase-plot (b)

As the airstream speed is further increased, the damping of the system keeps reducing; hence, the restoring forces are no longer able to limit the oscillations. Similarly to what happens in the flutter of linear systems, a divergent flapping motion is observed, as shown in Fig. 10(a). The curve in the phase portrait spirals away from the initial conditions, as shown in Fig. 10(b) at an airstream speed of $27\ \text{m}\,\text{s}^{-1}$. The divergent motion is in agreement with the positive LCEs shown in Fig. 6(d): largest two conjugate LCEs converge to a positive number.

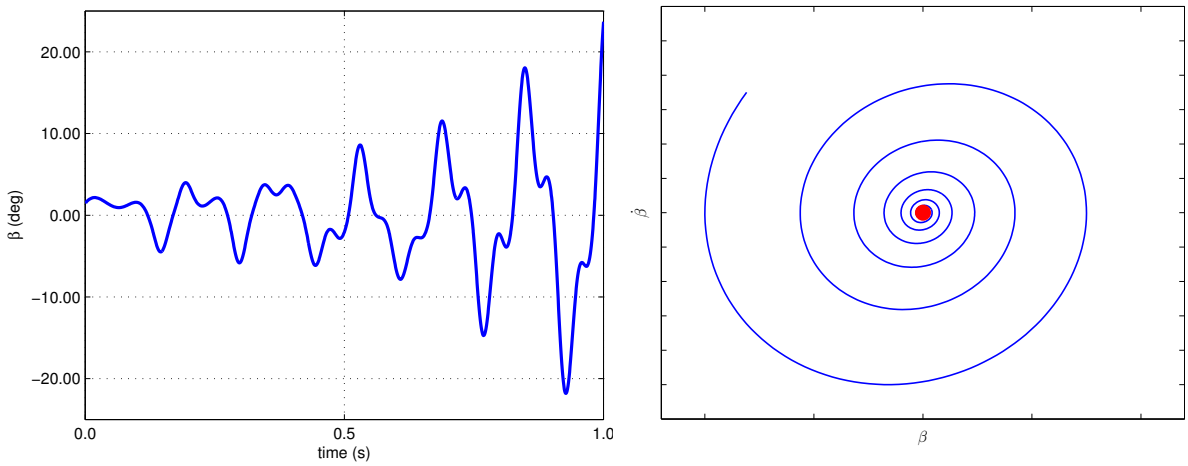

(a) time history (b) non-dimensional phase plot

Figure 10: Freeplay: aileron response at $U = 27\text{m}\,\text{s}^{-1}$; time history (a) and non-dimensional phase-plot (b)

4 CONCLUSIONS

A natural generalization of quantitative stability evaluation for aeroelastic problems with lumped nonlinearities in control surface is presented. The spectrum of the nonlinear aeroelastic problems is estimated using Lyapunov Characteristic Exponents. The Discrete QR algorithm has

been used for the practical estimation of Lyapunov Characteristic Exponents. The results are verified with time marching simulations of simplified aeroelastic problems.

LCEs correspond to the real part of the eigenvalues for Linear Time Invariant problems, and to Floquet multipliers for Linear Time Periodic problems; hence, they represent a natural generalization of stability indicators that are familiar in current engineering practice, including aeroelastic stability problems which involve nonlinearities of diverse origins. On the other hand, estimating LCEs is computationally more expensive than linear stability calculations and convergence can be problematic in case of paired LCEs related to same branch of solution. These drawbacks requires further research. However, as robust and cost efficient estimation algorithms are developed and verifications over more complex systems are performed, Lyapunov Characteristic Exponents can potentially be the standard stability evaluation practice for nonlinear aeroelastic problems.

5 REFERENCES

[1] Bisplinghoff, R. L., Ashley, H., and Halfman, R. L. (1996). *Aeroelasticity*. New York: Dover.

[2] Strogatz, S. H. (1994). *Nonlinear Dynamics and Chaos: With Applications to Physics, Biology, Chemistry, and Engineering*. Reading, Massachusetts: Perseus Books.

[3] Dowell, E., Edwards, J., and Strganac, T. (2003). Nonlinear aeroelasticity. *Journal of Aircraft*, 40(5), 857–874.

[4] Lee, B., Price, S., and Wong, Y. (1999). Nonlinear aeroelastic analysis of airfoils: bifurcation and chaos. *Progress in Aerospace Sciences*, 27, 205–334. doi:10.1016/j.paerosci.2009.08.002.

[5] Jinwu, X., Yongju, Y., and Daochun, L. (2014). Recent advance in nonlinear aeroelastic analysis and control of the aircraft. *Chinese Journal of Aeronautics*, 27(1), 12–22. doi:10.1016/j.cja.2013.12.009.

[6] Adrianova, L. Y. (1995). *Introduction to Linear Systems of Differential Equations*, vol. 146 of *Translations of Mathematical Monographs*. Providence, Rhode Island: American Mathematical Society.

[7] Benettin, G., Galgani, L., Giorgilli, A., et al. (1980). Lyapunov characteristic exponents for smooth dynamical systems and for Hamiltonian systems; a method for computing all of them. part 1: Theory. *Meccanica*, 15(1), 9–20. doi:10.1007/BF02128236.

[8] Dieci, L. and Van Vleck, E. S. (2002). Lyapunov and other spectra: a survey. In D. Estep and S. Taverner (Eds.), *Collected lectures on the preservation of stability under discretization*, chap. 11. Philadelphia, PA (USA): SIAM, pp. 197–218.

[9] Wolf, A., Swift, J. B., Swinney, H. L., et al. (1985). Determining Lyapunov exponents from a time series. *Physica D: Nonlinear Phenomena*, 16(3), 285–317. doi:10.1016/0167-2789(85)90011-9.

[10] Price, S. J., Ghanbari, H. A., and Lee, B. H. K. (1995). The aeroelastic response of a two dimensional airfoil with bilinear and cubic structural nonlinearities. *Journal of Fluids and Structures*, 9, 175–193.

[11] Dai, H., Yue, X., Xie, D., et al. (2014). Chaos and chaotic transients in an aeroelastic system. *Journal of Sound and Vibration*, 333, 7267–7285. doi:10.1016/j.jsv.2014.08.034.

[12] Liviu Librescu, P. M., Gianfranco Chiocchia (2003). Implications of cubic physical/aerodynamic non-linearities on the character of the flutter instability boundary. *International Journal of Non-Linear Mechanics*, 38(2), 173–199. doi:10.1016/S0020-7462(01)00054-3.

[13] Tamer, A. and Masarati, P. (2016). Stability of nonlinear, time-dependent rotorcraft systems using lyapunov characteristic exponents. *Journal of the American Helicopter Society*, 61(2), 14–23. .

[14] Masarati, P. and Tamer, A. (2015). Sensitivity of trajectory stability estimated by lyapunov characteristic exponents. *Aerospace Science and Technology*, 47, 501 – 510. doi: https://doi.org/10.1016/j.ast.2015.10.015.

[15] Cong, N. D. and Nam, H. (2003). Lyapunov's inequality for linear differential algebraic equation. *Acta Mathematica Vietnamica*, 28(1), 73–88.

[16] Cong, N. D. and Nam, H. (2004). Lyapunov regularity of linear differential algebraic equations of index 1. *Acta Mathematica Vietnamica*, 29(1), 1–21.

[17] Masarati, P. (2013). Estimation of Lyapunov exponents from multibody dynamics in differential-algebraic form. *Proc. IMechE Part K: J. Multi-body Dynamics*, 227(4), 23–33. doi:10.1177/1464419312455754.

[18] Geist, K., Parlitz, U., and Lauterborn, W. (1990). Comparison of different methods for computing Lyapunov exponents. *Progress of Theoretical Physics*, 83(5), 875–893. doi:10.1143/PTP.83.875.

[19] Masarati, P. and Tamer, A. (2016). The real schur decomposition estimates lyapunov characteristic exponents with multiplicity greater than one. *Proceedings of the Institution of Mechanical Engineers, Part K: Journal of Multi-body Dynamics*, 230(4), 568–578. doi: 10.1177/1464419316637275.

[20] Edwards, J. W., Ashley, H., and Breakwell, J. V. (1979). Unsteady aerodynamic modeling for arbitrary motions. *AIAA Journal*, 17(4), 365–374. doi:10.2514/3.7348.

[21] Theodorsen, T. and Garrick, I. (1942). Nonstationary flow about a wing-aileron-tab combination including aerodynamic balance. Report 736, NACA.

[22] Lee, B. H. K., Jiang, L., and Wong, Y. S. (1999). Flutter of an airfoil with a cubic restoring force. *Journal of Fluids and Structures*, 13, 75–101. doi:10.1016/j.jfluidstructs.2007.08.003.

[23] Li, D., Guo, S., and Xiang, J. (2010). Aeroelastic dynamic response and control of an airfoil section with control surface nonlinearities. *Journal of Sound and Vibration*, 329, 4756–4771. doi:10.1016/j.jsv.2010.06.006.

[24] Abdelkefi, A., Vasconcellos, R., Nayfeh, A. H., et al. (2013). An analytical and experimental investigation into limit-cycle oscillations of an aeroelastic system. *Nonlinear Dynamics*, 71, 159–173. doi:10.1007/s11071-012-0648-z.

[25] Lee, B., Liu, L., and Chung, K. (2005). Airfoil motion in subsonic flow with strong cubic nonlinear restoring forces. *Journal of Sound and Vibration*, 281, 699–717. 10.1016/j.jsv.2004.01.034.

[26] Medio, A. and Lines, M. (2001). *Nonlinear Dynamics — A Primer*. Cambridge University Press.

[27] Eller, D. (2007). Friction, freeplay and flutter of manually controlled aircraft. In *International Forum on Aeroelasticity and Structural Dynamics*. Stockholm, Sweden.

[28] Liu, L. and Dowell, E. H. (2005). Harmonic balance approach for an airfoil with a freeplay control surface. *AIAA Journal*, 43(4), 802–815. doi:10.2514/1.10973.

[29] Vasconcellos, R., Abdelkefi, A., Marques, F., et al. (2012). Representation and analysis of control surface freeplay nonlinearity. *Journal of Fluids and Structures*, 31, 79–91. doi:10.1016/j.jfluidstructs.2012.02.003.

[30] Vasconcellos, R., Abdelkefi, A., Hajj, M. R., et al. (2013). Discontinuity induced bifurcation in aeroelastic systems with freeplay nonlinearity. In *22nd International Congress of Mechanical Engineering (COBEM'13)*. Ribeirao Preto, SP, Brasil, pp. 2832–2843.

[31] M.D. Conner, E. D. L. V., D.M. Tang (1997). Nonlinear behavior of a typical airfoil section with control surface freeplay: a numerical and experimental study. *Journal of Fluids and Structures*, 11, 89–109.

COPYRIGHT STATEMENT